THE JOURNAL OF BIOLOGICAL CHEMISTRY VOL. 291, NO. 31, pp. 16038–16047, July 29, 2016

OxyR2 Functions as a Three-state Redox Switch to Tightly Regulate Production of Prx2, a Peroxiredoxin of *Vibrio vulnificus*[*]

Received for publication, December 13, 2015, and in revised form, June 2, 2016 Published, JBC Papers in Press, June 6, 2016, DOI 10.1074/jbc.M115.710343

Ye-Ji Bang[‡§], Zee-Won Lee[‡§], Dukyun Kim[‡§], Inseong Jo[§], Nam-Chul Ha[§1], and Sang Ho Choi[‡§2]

From the [‡]National Research Laboratory of Molecular Microbiology and Toxicology and the [§]Department of Agricultural Biotechnology, and Center for Food Safety and Toxicology, Seoul National University, Seoul 08826, Korea

The bacterial transcriptional regulator OxyR is known to function as a two-state redox switch. OxyR senses cellular levels of H_2O_2 via a "sensing cysteine" that switches from the reduced to a disulfide state upon H_2O_2 exposure, inducing the expression of antioxidant genes. The reduced and disulfide states of OxyR, respectively, bind to extended and compact regions of DNA, where the reduced state blocks and the oxidized state allows transcription and further induces target gene expression by interacting with RNA polymerase. *Vibrio vulnificus* OxyR2 senses H_2O_2 with high sensitivity and induces the gene encoding the antioxidant Prx2. In this study, we used mass spectrometry to identify a third redox state of OxyR2, in which the sensing cysteine was overoxidized to *S*-sulfonated cysteine (Cys-SO_3H) by high H_2O_2 *in vitro* and *in vivo*, where the modification deterred the transcription of *prx2*. The DNA binding preferences of OxyR2$_{5CA}$-C206D, which mimics overoxidized OxyR2, suggested that overoxidized OxyR2 binds to the extended DNA site, masking the −35 region of the *prx2* promoter. These combined results demonstrate that OxyR2 functions as a three-state redox switch to tightly regulate the expression of *prx2*, preventing futile production of Prx2 in cells exposed to high levels of H_2O_2 sufficient to inactivate Prx2. We further provide evidence that another OxyR homolog, OxyR1, displays similar three-state behavior, inviting further exploration of this phenomenon as a potentially general regulatory mechanism.

Reactive oxygen species build up as metabolic by-products from oxygen during aerobic respiration processes (1, 2). Of the reactive oxygen species, hydrogen peroxide (H_2O_2) is toxic to cellular components, especially when it is converted to the hydroxyl radical via the Fenton reaction in the presence of iron or copper ions (3, 4). Pathogenic bacteria inevitably encounter elevated levels of H_2O_2 imposed by the host immune response system during infection. Therefore, pathogenic bacteria have to cope with H_2O_2 to survive host environments and in turn to ensure developing illness. Therefore, the bacteria's mechanisms to defense against H_2O_2 are closely linked to their virulence (5). Bacterial defense against H_2O_2 relies on a variety of antioxidant defense enzymes, such as peroxiredoxins (Prxs)[3] and catalases (6).

OxyR is a central regulator of the antioxidant genes in many bacteria and forms a homotetramer (7). OxyR is a modular structure consisting of an N-terminal DNA binding domain and C-terminal regulatory domain that contains two conserved redox-sensitive cysteines. Typical OxyR, such as *Escherichia coli* OxyR, has been considered as a "two-state redox switch" that precisely modulates expression of many antioxidant genes in a H_2O_2-dependent manner (7–9). When H_2O_2 is low and within safe limits, the redox-sensitive cysteines are present as free thiols separated by an α-helix, resulting in the "reduced state" of OxyR. In the reduced state, the OxyR tetramer adopts an extended conformation (10) and binds to the extended DNA-binding sites to mask the −35 region of the target antioxidant genes (11, 12). Thereby, the reduced OxyR turns off the expressions of target antioxidant genes under conditions of low H_2O_2 (12–14). When H_2O_2 increases and exceeds safe limits, one of the redox-sensitive cysteines, named sensing cysteine, senses H_2O_2 and is rapidly oxidized to Cys-SOH (15). Given the high reactivity, the Cys-SOH readily forms an intramolecular disulfide bond (Cys-S-S-Cys) with the other redox-sensitive cysteine. This "oxidized state or disulfide state" of OxyR adopts compact conformation, binds to more compact DNA-binding sequences, and unmasks the −35 region (11, 12). The oxidized OxyR interacts with the C-terminal domain of RNA polymerase α-subunits and turns on the target antioxidant genes under conditions of high H_2O_2 (8, 12, 16).

The facultative aerobic pathogen *Vibrio vulnificus* has two OxyRs, OxyR1 and OxyR2 (11). Amino acid sequences of both OxyR proteins have the conserved residues that are functionally important in OxyR, indicating that OxyR1 and OxyR2 share common functional and structural characteristics with the OxyR homologs of many bacteria. OxyR1 and OxyR2 activate *prx1* and *prx2*, respectively (11). Each of the Prxs scavenges distinct ranges of H_2O_2 (*i.e.* working ranges of H_2O_2 for each Prx). Prx2 has a higher affinity for H_2O_2 than Prx1 and thus scavenges lower levels of H_2O_2 more effectively, whereas Prx1 detoxifies higher levels of H_2O_2 more effectively. It is notewor-

[*] This work was supported by Mid-career Researcher Program Grant 2015R1A2A1A13001654 through the National Research Foundation, funded by the Ministry of Science, ICT, and Future Planning (to S. H. C.) and the R&D Convergence Center Support Program of the Ministry of Agriculture, Food, and Rural Affairs (to S. H. C. and N.-C. H.), Republic of Korea. The authors declare that they have no conflicts of interest with the contents of this article.

[1] To whom correspondence may be addressed. Tel.: 82-2-880-4853; Fax: 82-2-873-5095; E-mail: hanc210@snu.ac.kr.

[2] To whom correspondence may be addressed. Tel.: 82-2-880-4857; Fax: 82-2-873-5095; E-mail: choish@snu.ac.kr.

[3] The abbreviations used are: Prx, peroxiredoxin; AMS, 4-acetamido-4′-maleimidylstilbene-2, 2′-disulfonic acid.

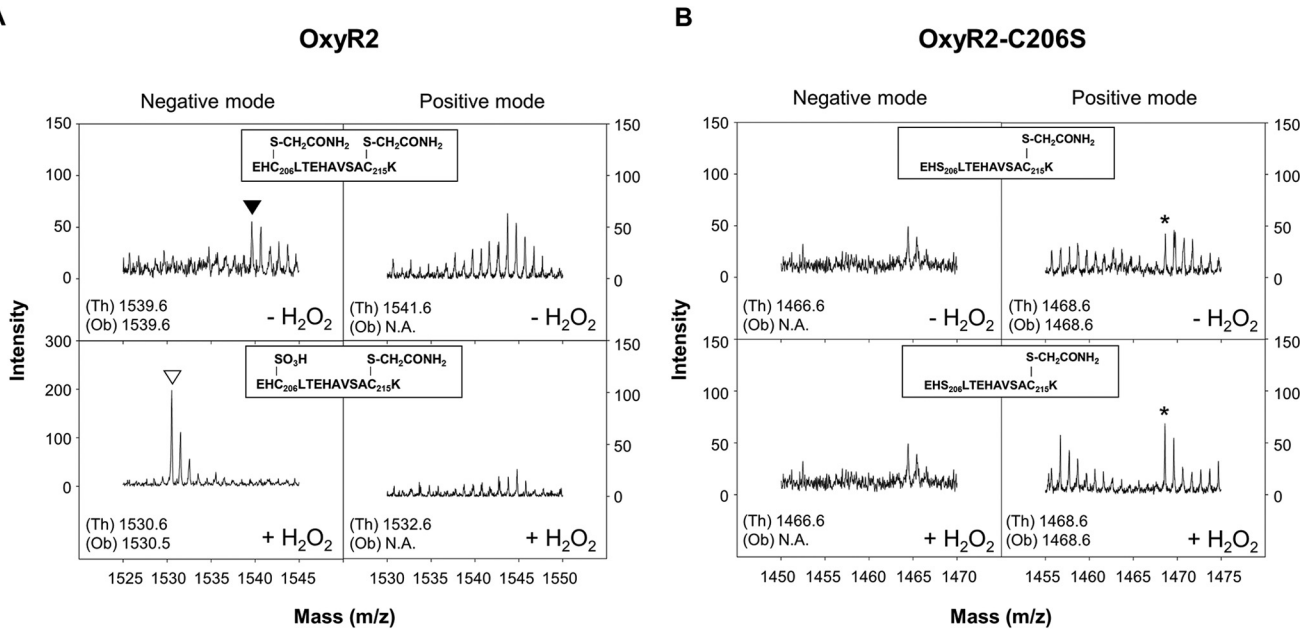

FIGURE 1. **MALDI-TOF mass spectra of OxyR2 and OxyR2-C206S oxidized by 500 μM H_2O_2 *in vitro*.** His_6-tagged OxyR2 (*A*) and OxyR2-C206S (*B*) proteins were reduced with 100 mM DTT for 1 h and desalted by gel filtration chromatography under anaerobic conditions. Then the OxyR2 proteins were reacted (*bottom panels*, $+H_2O_2$) or unreacted (*top panels*, $-H_2O_2$) with 500 μM H_2O_2 for 10 min. Each of the OxyR2 proteins was then incubated with iodoacetamide to alkylate reduced cysteine residues, digested with trypsin, and analyzed by MALDI-TOF MS in negative (*left panels*) and positive (*right panels*) ion reflector modes. *A*, mass spectra of peptides containing Cys^{206} of OxyR2 are indicated. ▼, a peptide with alkylated Cys^{206} and Cys^{215}; ▽, a peptide with *S*-sulfonated Cys^{206} and alkylated Cys^{215}. *B*, mass spectra of peptides containing Ser^{206} of OxyR2-C206S are indicated. *, a peptide with alkylated Cys^{215}. The form of each observed peptide is indicated in the *box inside* each *panel*. Theoretical (*Th*) and observed (*Ob*) monoisotopic masses ($[M - H]^-$ for negative mode or $[M + H]^+$ for positive mode) of the peptides are indicated in the *bottom left corner* of each *panel*. *N.A.*, the corresponding peptide was not observed.

thy that Prx2 is sensitive, whereas Prx1 is relatively robust, to H_2O_2. Prx2 is irreversibly inactivated by overoxidation at one of the catalytic cysteines, peroxidatic cysteine, to *S*-sulfonated cysteine (Cys-SO_3H) in cells exposed to 30 μM or higher levels of H_2O_2 that exceed its working range (17).

This observation led us to raise a question on the redox state and transcriptional activity of OxyR2 in the cells in which cellular H_2O_2 level is high enough to irreversibly inactivate Prx2. Accordingly, the present study examined the redox state of OxyR2 exposed to various levels of H_2O_2 *in vivo* as well as *in vitro*. MS analysis found that the sensing cysteine is overoxidized to Cys-SO_3H by high H_2O_2 *in vitro*. The "overoxidized state" is a third redox state in addition to the reduced and disulfide states of OxyR2. We confirmed the presence of the overoxidized state of OxyR2 in *V. vulnificus* cells exposed to H_2O_2 exceeding 30 μM. Biochemical and genetic studies demonstrated that the overoxidized OxyR2 deters the production of Prx2 that is no longer functional. The sequences for binding of the overoxidized OxyR2 were determined to explain the mechanism of overoxidized OxyR2 to turn off the *prx2* expression. Finally, the possibility that the OxyR1 is also overoxidized to play a role in the regulation of its antioxidant genes was investigated.

Results

Sensing Cysteine of OxyR2 Is Overoxidized at High Levels of H_2O_2—The purified OxyR2 protein was reacted with 500 μM H_2O_2 *in vitro*, and the redox state of the sensing cysteine Cys^{206} was subjected to MALDI-TOF MS analysis in positive and negative ion reflector modes (Fig. 1). Peptides can be detected in positive and/or negative ion reflector modes, depending on the intrinsic properties of the peptides that influence the ionization behavior (18). Mass spectra for the tryptic digests of the OxyR2 protein were analyzed after the free cysteine residues in the sample were alkylated with iodoacetamide to prevent further oxidation during the analysis. As shown in Fig. 1*A*, the peptide fragment containing both redox-sensitive cysteine residues ($EHC^{206}LTEHAVSAC^{215}K$) was detectable in the negative ion reflector mode. It remained reduced in the absence of H_2O_2 and thus produced the doubly alkylated version (Cys-S-CH_2CONH_2) with a monoisotopic mass $[M - H]^-$ of 1539.6 (Fig. 1*A*, *top*). However, upon reaction with 500 μM H_2O_2, the monoisotopic mass $[M - H]^-$ of the peptide fragment decreased to 1530.5, suggesting that the peptide fragment contains one *S*-sulfonated cysteine (Cys-SO_3H) and one alkylated cysteine. The peptide fragment with *S*-sulfinated cysteine (Cys-SO_2H; $[M - H]^-$ of 1514.6 or $[M + H]^+$ of 1516.6) was not observed under the experimental conditions we tested (data not shown). The $EHC^{206}LTEHAVSAC^{215}K$ peptide fragment was not detectable in the positive ion mode regardless of H_2O_2 treatment (Fig. 1*A*, *right panels*).

To determine which cysteine residue was *S*-sulfonated by H_2O_2, the same analysis with the OxyR2-C206S variant was performed in the absence and presence of 500 μM H_2O_2. The tryptic peptide fragment ($EHS^{206}LTEHAVSAC^{215}K$) was detected in the positive ion reflector mode and had a singly alkylated protein at Cys^{215} showing the monoisotopic mass $[M + H]^+$ of 1468.6 regardless of the presence of H_2O_2 (Fig. 1*B*, *right panels*). Neither peptide fragment with Cys^{215}-SO_3H ($[M + H]^+$ of 1459.6 or $[M - H]^-$ of 1457.6) nor with Cys^{215}-SO_2H ($[M + H]^+$ of 1443.6 or $[M - H]^-$ of 1441.6) was found,

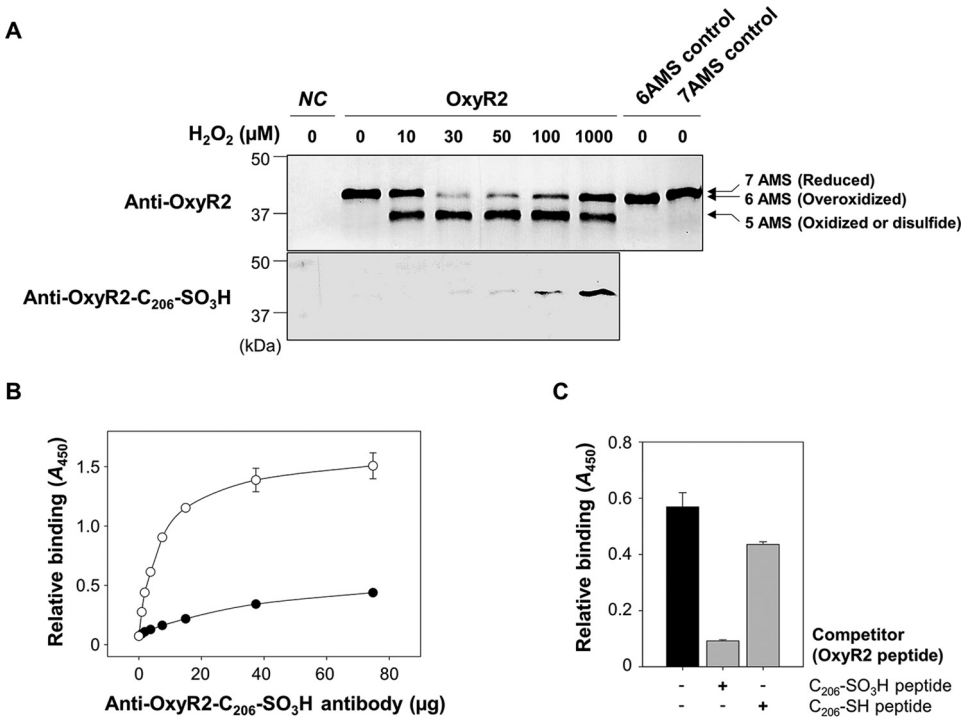

FIGURE 2. **Overoxidation of OxyR2 Cys^{206} in *V. vulnificus* cells exposed to various levels of H_2O_2.** *A*, OH0703 (pDY1025) was grown anaerobically to an A_{600} of 0.3 and exposed to various H_2O_2 concentrations for 3 min. Cellular proteins were precipitated with TCA and alkylated with fresh AMS buffer for 1 h at 37 °C. Proteins (3.5 μg for the *top panel* and 7 μg for the *bottom panel*) were resolved by non-reducing SDS-PAGE and immunoblotted using anti-OxyR2 antibody (*top*) or anti-OxyR2-Cys^{206}-SO_3H antibody (*bottom*). The predicted numbers of AMS that alkylated each OxyR2 molecule and their redox states are indicated at the *ends* of the gel. Negative control (*NC*) was OH0703 (pJH0311), 6AMS control was OH0703 (pBANG1416), and 7AMS control was OH0703 (pDY1025). *B*, the specificity of anti-OxyR2-Cys^{206}-SO_3H antibody to overoxidized and reduced OxyR2 was determined using ELISA. The microtiter 96-well plates were coated with 0.1 μg of synthetic peptides corresponding to either OxyR2 active site with overoxidized (*S*-sulfonated) Cys^{206} (EKEHC^{206}(SO_3H)LTEHA) (○) or with reduced Cys^{206} (EKEHC^{206}(SH)LTEHA) (●), and the peptides were reacted with various concentrations of the antibody as indicated. *C*, the *S*-sulfonated OxyR2 peptide (0.1 μg) was attached to the microtiter 96-well plates and then reacted with 4 μg of anti-OxyR2-Cys^{206}-SO_3H antibody. As a binding competitor, either *S*-sulfonated or reduced OxyR2 peptides (12.5 ng) were added to the reaction with the antibody as indicated. *Black bar*, control where no competitor was added. Relative binding of the antibody to the specific peptides is presented as A_{450}. All data in *B* and *C* represent mean ± S.D. (*error bars*).

indicating that Cys^{215} did not undergo the overoxidation. The EHS^{206}LTEHAVSAC^{215}K peptide fragment was not detectable in the negative ion mode (Fig. 1*B*, *left panels*). Therefore, the combined results demonstrated that the sensing cysteine, Cys^{206}, but not the other cysteine, Cys^{215}, of OxyR2 is overoxidized to Cys-SO_3H in the presence of high levels of H_2O_2 *in vitro*.

Overoxidation of OxyR2 in the V. vulnificus Cells Exposed to H_2O_2—To ascertain whether the overoxidation of OxyR2 at the sensing cysteine indeed occurs by cellular H_2O_2 in *V. vulnificus*, the redox state of cellular OxyR2 was analyzed. The *oxyR2* mutant OH0703 with pDY1025 expressing *oxyR*2 was grown anaerobically, exposed to various concentrations of H_2O_2, and then treated with 0.5-kDa 4-acetamido-4′-maleimidylstilbene-2, 2′-disulfonic acid (AMS; Invitrogen) to alkylate free thiols in the proteins. The total cellular proteins (3.5 μg/well) were resolved on non-reducing SDS-PAGE and immunoblotted with anti-OxyR2 antibody. Alkylation of a free thiol in the proteins with AMS adds 0.5 kDa of molecular mass (Fig. 2*A*, *top*). OxyR2 in the cells without exposure to H_2O_2 existed in the reduced state in which all seven cysteine residues present in OxyR2 were alkylated with AMS (7AMS control). An OxyR2 band containing pentuply alkylated cysteine residues coexisted with the heptuply alkylated OxyR2 band when the cells were exposed to 10 μM H_2O_2, indicating that a part of OxyR2 was oxidized to form a disulfide bond, as observed in the previous report (11). More importantly, a portion of OxyR2 in the cells exposed to H_2O_2 exceeding 30 μM appeared to have sextuply alkylated cysteine residues, indicating that one of the seven cysteine residues of OxyR2 had a single modification, such as an oxidation, that could prevent alkylation by AMS. When determined based on the band intensities, relative amounts of the OxyR2 with the single cysteine modification (or sextuply alkylated) were increased gradually by exposure to higher levels of H_2O_2 (Fig. 2*A*, *top*).

To examine whether the OxyR2 with a single cysteine modification observed in the cells exposed to H_2O_2 exceeding 30 μM is the OxyR2 with overoxidized Cys^{206}, the total cellular proteins (7.0 μg/well) were resolved on non-reducing SDS-PAGE and immunoblotted with the anti-OxyR2-Cys^{206}-SO_3H antibody (Fig. 2*A*, *bottom*). The OxyR2 protein with overoxidized Cys^{206} was specifically detected in cells exposed to H_2O_2 exceeding 30 μM and increased gradually in the cells exposed to higher levels of H_2O_2. The results indicated that the sensing cysteine of OxyR2 becomes overoxidized *in vivo* when the *V. vulnificus* cells are exposed to high levels of H_2O_2, as was demonstrated *in vitro* (Fig. 1).

Concurrently, to determine the specificity of the anti-OxyR2-Cys^{206}-SO_3H antibody by ELISA, the antibody was tested to react with the Cys^{206}-SO_3H or Cys^{206}-SH peptides that were synthesized and attached to the microtiter 96-well plates. The antibody specifically bound to the Cys^{206}-SO_3H

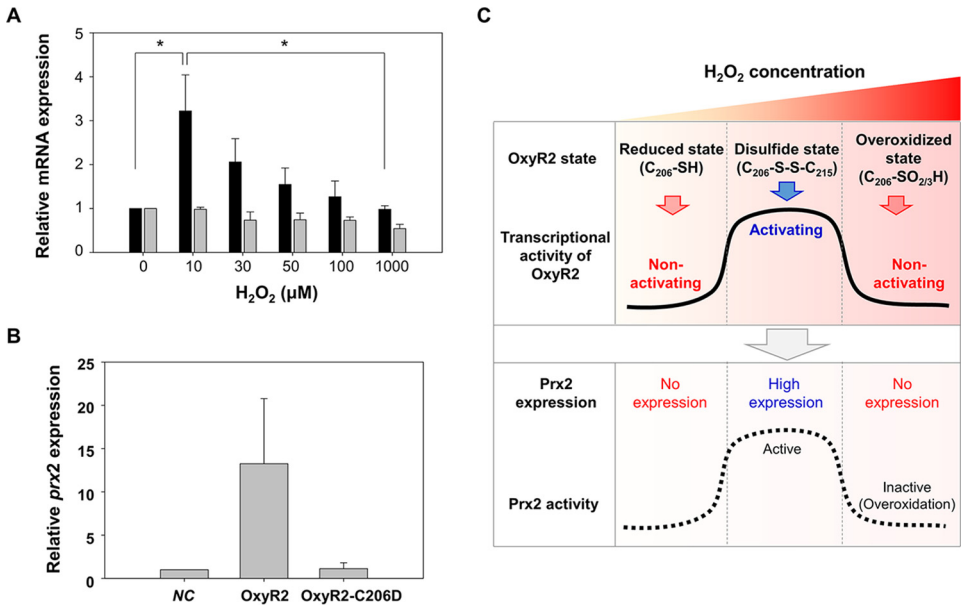

FIGURE 3. **Expression levels of *prx2* in response to various levels of H_2O_2 and a working model for OxyR2 as a three-state redox switch.** *A*, wild-type *V. vulnificus* was grown anaerobically to an A_{600} of 0.3 and exposed to various concentrations of H_2O_2 as indicated for 3 min. Total RNAs were isolated, and the relative levels of *prx2* (*black bars*) and *oxyR2* (*gray bars*) transcripts were determined by quantitative real-time PCR analyses. The level of each transcript from wild type unexposed to H_2O_2 is presented as 1. *, statistically significant difference ($p < 0.05$) between groups. *B*, transcriptional activity of OxyR2-C206D. Cultures were grown aerobically to an A_{600} of 0.5, total RNAs were isolated, and the relative levels of *prx2* transcript were determined by quantitative real-time PCR analyses. The level of transcript from negative control (*NC*) is presented as 1. Negative control was OH0703 (pJH0311). *OxyR2*, OH0703 (pDY1025); *OxyR2-C206D*, OH0703 (pBANG1416). All data in *A* and *B* represent mean ± S.D. (*error bars*). *C*, OxyR2 shifts to three different redox states, revealing different transcriptional activities in response to various levels of H_2O_2 in cells (*solid line*) as indicated. Concurrently, the *prx2* expression (*dotted line*) varies, depending on the redox states of OxyR2. *C_{206}-$SO_{2/3}$H*, overoxidized Cys^{206} with Cys^{206}-SO_2H and/or Cys^{206}-SO_3H.

peptide (Fig. 2*B*). Furthermore, the binding of the antibody to the attached Cys^{206}-SO_3H peptide was effectively inhibited by the Cys^{206}-SO_3H peptide added to the reaction as a competitor (Fig. 2*C*). The antibody slightly bound to the Cys^{206}-SH peptide (Fig. 2*B*), and the Cys^{206}-SH peptide competitor could marginally inhibit the antibody reaction to the Cys^{206}-SO_3H peptide (Fig. 2*C*), reflecting that Cys^{206}-SH peptide could be oxidized to Cys^{206}-SO_3H peptide in the aerobic conditions we tested. The results indicated that the anti-OxyR2-Cys^{206}-SO_3H antibody we used is specific to the OxyR2 with Cys^{206}-SO_3H. However, it was not possible to examine the antibody's specificity to Cys^{206}-SO_2H. Therefore, the OxyR2 with Cys^{206}-$SO_{2/3}$H is hereafter designated as the overoxidized state of OxyR2.

Overoxidized State of OxyR2 Turns Off the prx2 Promoter—To examine the transcriptional activity of the overoxidized state of OxyR2, the expression of *prx2* was monitored in the wild-type *V. vulnificus* cells. The expression of *prx2* was significantly induced when the anaerobically grown cells were exposed to 10 μM H_2O_2 (Fig. 3*A*), indicating that OxyR2 was oxidized to the disulfide state under this condition to activate the *prx2* promoter (P_{prx2}) (Fig. 2*A*). However, the level of *prx2* transcript gradually decreased along with increasing concentrations of H_2O_2 exceeding 30 μM (Fig. 3*A*), which was in accordance with the increase of the overoxidized state of OxyR2 (Fig. 2*A*). The changes in *prx2* expression were dependent on OxyR2 activity, but not on *oxyR2* expression level, because the expression level of *oxyR2* was not significantly affected by increasing concentrations of H_2O_2 below 1 mM (Fig. 3*A*). The combined results suggested that the overoxidized state of OxyR2 deters further expression of *prx2*. Because it has been reported that Prx2 is inactivated by H_2O_2 exceeding 30 μM (17), this deterrence of the *prx2* expression may prevent the worthless production of Prx2 in the environments of high H_2O_2, where Prx2 is no longer functional.

However, it was still possible that H_2O_2 over 30 μM can also detrimentally affect other transcription factors, such as components of RNA polymerase, to deter the *prx2* expression. To rule out this possibility, OH0703 containing pBANG1416 expressing OxyR2-C206D was grown aerobically without exogenously added H_2O_2, and the *prx2* expression was compared. It has been reported that the size and the polar properties of aspartic acid are comparable with those of the overoxidized cysteine residues (Cys-SO_2H and Cys-SO_3H), and therefore OxyR2-C206D is anticipated to mimic the overoxidation state of OxyR2 (10). As shown in Fig. 3*B*, OH0703 producing wild-type OxyR2 expressed almost 13-fold greater *prx2* than the negative control strain lacking OxyR2. This supported our previous observation that wild-type OxyR2 activates the *prx2* expression under aerobic conditions (11). In contrast, the *prx2* expression level of the strain producing OxyR2-C206D was almost the same as that of the negative control strain (Fig. 3*B*). The results indicated that the deterrence of the *prx2* expression in response to H_2O_2 exceeding 30 μM is caused mainly, if not solely, by overoxidation of OxyR2 and further confirmed that OxyR2-C206D is functionally similar to the overoxidized OxyR2.

OxyR2 Regulates prx2 as a Three-state Redox Switch in Response to H_2O_2—Fig. 3*C* represents the working model of OxyR2 that regulates the expression of *prx2* as a three-state redox switch. OxyR2 adopts the three distinct redox states (reduced state, disulfide state, and overoxidized state) in an H_2O_2 concentration-dependent manner (Figs. 1 and 2). So far in the widely accepted mechanism of OxyR proteins, OxyR2

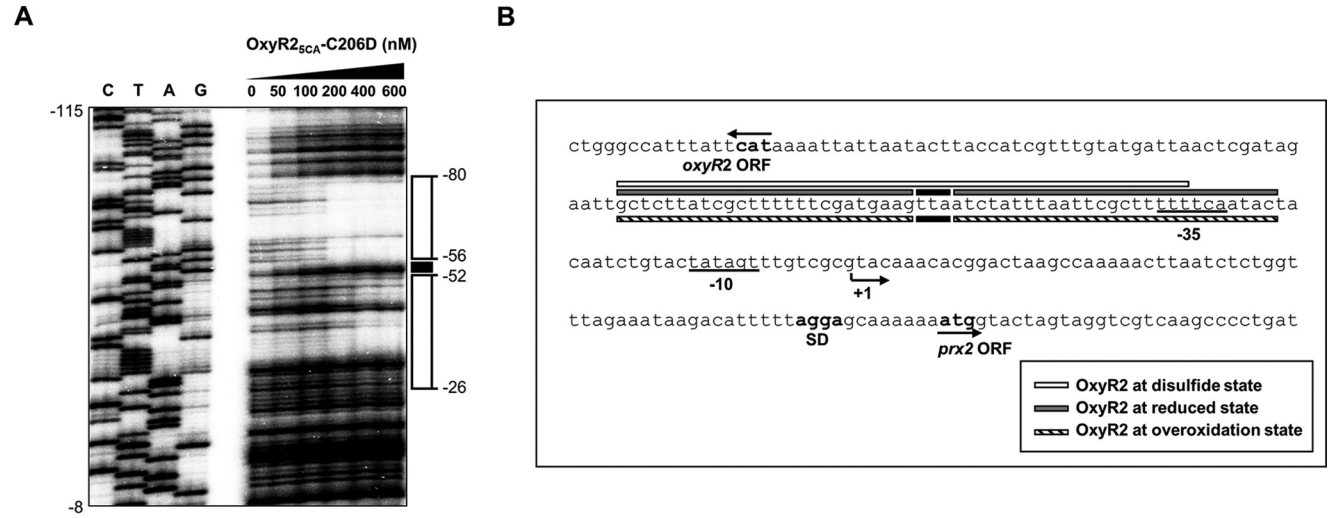

FIGURE 4. **Binding sequences of OxyR2$_{5CA}$-C206D within the *prx2* promoter region.** *A*, a 260-bp DNA fragment of the upstream region of P_{prx2} was radioactively labeled and then used as probe DNA. The radiolabeled probe DNA (25 nM) was incubated with increasing amounts of the purified OxyR2$_{5CA}$-C206D as indicated and then digested with DNase I. The regions protected by OxyR2$_{5CA}$-C206D are indicated by *open boxes*, whereas the nucleotides showing enhanced cleavage are indicated by a *black box*. *Lanes C*, *T*, *A*, and *G*, nucleotide sequencing ladder of P_{prx2}. *Nucleotide numbers* shown are relative to the transcription start site of P_{prx2}. *B*, the sequences for binding of OxyR2$_{5CA}$-C206D are indicated *below* the P_{prx2} sequences as *diagonal-filled boxes*. The sequences for binding of oxidized OxyR2 (*white box*) and reduced OxyR2 (*gray boxes*) determined previously (11) are presented *above* the P_{prx2} sequences. The nucleotides showing enhanced cleavage by binding of OxyR2$_{5CA}$-C206D and the reduced OxyR2 are indicated as *black boxes*. The transcription start site of P_{prx2} identified previously (11) is indicated by a *bent arrow*, and the positions of the putative −10 and −35 regions are *underlined*. The ATG translation initiation codon and the putative ribosome-binding site (*SD*) are also indicated in *boldface type*.

shifts its redox state from the reduced state to the disulfide state upon reaction with H_2O_2 and activates the expression of *prx2*. However, when exposed to H_2O_2 exceeding the working range for Prx2, OxyR2 moves to an overoxidized state, a third redox state, and turns off the expression of *prx2*. It is obvious that OxyR2 is able to prevent production of useless Prx2 and thus save valuable cellular resources by working as a three-state redox switch (Fig. 3*C*).

Mechanism of the Overoxidized OxyR2 to Turn Off P_{prx2}—To gain insight into the mechanism by which the overoxidized state of OxyR2 deters the expression of *prx2*, the sequences for binding of the overoxidized OxyR2 were determined. Purified OxyR2$_{5CA}$-C206D, which mimics overoxidized OxyR2 and is soluble under aerobic conditions, was used *in vitro* for the DNA footprinting assay. OxyR2$_{5CA}$, in which all five non-catalytic cysteine residues in OxyR2 were replaced with alanine residues, was constructed previously (11). The purified OxyR2$_{5CA}$ did not form oligomers *in vitro* under nonreducing conditions (11). As shown in Fig. 4, the sequences for binding of OxyR2$_{5CA}$-C206D were extended from −80 to −26 relative to the transcription start site of P_{prx2}. Therefore, one possible mechanism is that the overoxidized OxyR2 presumably turns off the expression of *prx2* by masking the −35 region and thereby preventing RNA polymerase binding to P_{prx2}.

Furthermore, the binding sequences of OxyR2$_{5CA}$-C206D are identical to those of the reduced OxyR2. Enhanced cleavage in several nucleotides (−53 to −55), which was observed in the binding sequences of the reduced OxyR2, was also found in the binding sequences of OxyR2$_{5CA}$-C206D (Fig. 4*B*). It has been proposed that OxyR tetramer in the reduced state adopts an extended conformation (10) and binds to the elongated DNA-binding sites (11, 12). The combined results suggest that the overoxidized state of OxyR2 turns off the activation of *prx2* by adopting a conformation similar to that of the reduced state, binding to the elongated sequences, and preventing RNA polymerase binding to the promoter sequences.

Possible Overoxidation of OxyR1—To probe whether other OxyR proteins could function as a three-state redox switch, the expression of *prx1* and *katG* in the *V. vulnificus* cells exposed to various levels of H_2O_2 was determined (Fig. 5, *A* and *B*). It has been reported that OxyR1, a homolog of *E. coli* OxyR, directly activates the expression of *prx1* and *katG* (11).[4] Expression of both antioxidant genes in *V. vulnificus* increased along with increasing levels of H_2O_2 but decreased when H_2O_2 levels exceeded certain levels; the expression levels of *prx1* and *katG* showed the highest peaks in cells exposed to 30 and 10 μM H_2O_2, respectively, and then decreased in cells exposed to higher levels of H_2O_2 (Fig. 5, *A* and *B*). This variation of the *prx1* and *katG* expression in response to increasing levels of H_2O_2 was similar to that of the *prx2* expression (Fig. 3*A*), indicating that OxyR1 was also probably overoxidized to turn off expression of *prx1* and *katG* when the H_2O_2 levels exceeded the working ranges for Prx1 and KatG. This result suggested that OxyR homologs of other bacteria could function as a three-state redox switch to tightly regulate their target antioxidant genes.

Discussion

In this study, we present evidence that *V. vulnificus* OxyR2 regulates the expression of *prx2* as a three-state redox switch. When OxyR2 encountered H_2O_2 exceeding the Prx2 working range, the sensing cysteine of OxyR2 was overoxidized to Cys^{206}-SO_3H *in vivo* as well as *in vitro* (Figs. 1 and 2). Although MS analysis was unable to detect the peptide fragment of OxyR2 with Cys^{206}-SO_2H (Fig. 1*A*), the *S*-sulfinated form of OxyR2 was most likely formed as an intermediate in the course of the overoxidation of OxyR2 to the *S*-sulfonated OxyR2 (19).

[4] S. H. Choi, unpublished observation.

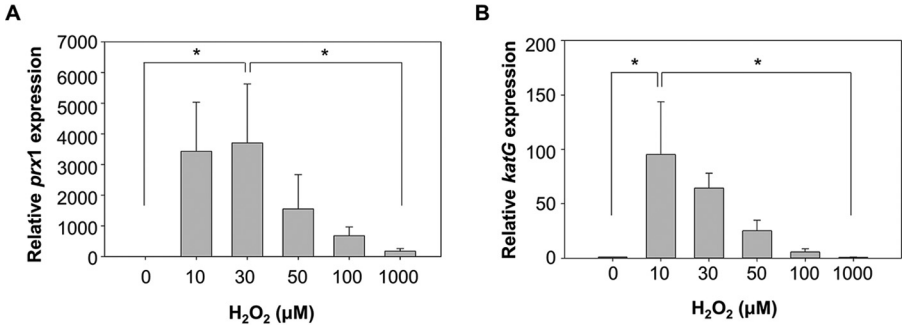

FIGURE 5. **Expression levels of *prx1* and *katG* in response to various levels of H_2O_2.** Wild-type *V. vulnificus* was grown anaerobically to an A_{600} of 0.3 and exposed to various concentrations of H_2O_2 as indicated for 3 min. Total RNAs were isolated, and the relative levels of *prx1* (*A*) and *katG* (*B*) transcripts were determined by quantitative real-time PCR analyses. The level of each transcript from wild type unexposed to H_2O_2 is presented as 1. *, statistically significant difference ($p < 0.05$) between groups. All data represent mean ± S.D. (*error bars*).

In addition to the reduced and oxidized (disulfide) states, the overoxidized state is the third redox state of OxyR2, whose function was primarily characterized in this study. The overoxidized OxyR2 actively turns off the transcription of *prx2* by binding to elongated sequences masking the −35 region of P_{prx2} in the environments of high H_2O_2, where Prx2 is no longer functional (Figs. 3 and 4) (17). Obviously, the overoxidized OxyR2 can prevent production of useless Prx2 and thus save valuable cellular resources. Therefore, the overoxidized OxyR2 is not simply an expired or perished form of OxyR2 but rather plays an important role in the survival of *V. vulnificus* during pathogenesis.

It was noteworthy that expression of *prx1* and *katG* was increased, reached a maximum, and then was decreased by exposure of cells to increasing levels of H_2O_2 in a pattern similar to that of *prx2* (Fig. 5, *A* and *B*). Both *prx1* and *katG* are regulated by OxyR1, a homolog of *E. coli* OxyR (11), implying that OxyR2 is not the only OxyR regulating antioxidant genes as a three-state redox switch. OxyR has been primarily thought of as a two-state redox switch that turns the antioxidant genes off and on in an H_2O_2-dependent manner (7–9). When bacteria encounter manageable ranges of H_2O_2, OxyR turns on its target genes encoding antioxidants, such as Prxs and catalases. Scavenging the H_2O_2 using the antioxidants and maintaining metabolic activities to keep growing is beneficial for bacteria. Accordingly, expression of most of the OxyR regulon is governed by the housekeeping σ factor RpoD (σ^{70}) (20). However, when H_2O_2 exceeds the manageable ranges, maintaining expressions of the antioxidant genes would be worthless because growth and proliferation of bacterial cells under this condition could be reckless. Instead, bacteria rather express many stress tolerance genes governed by the stress-responsive σ factor RpoS (σ^{38}) and shift their global physiology to stationary (or dormant) phase (21, 22). Bacteria can turn off the antioxidant genes using OxyR, as a three-state redox switch, under conditions in which expression of the antioxidants is useless. It is obviously advantageous that bacteria utilize more cellular resources to express stress tolerance genes encoding many additional protective systems (20, 21).

The mechanism for the overoxidation of the sensing cysteine remains unclear. However, structural analysis of the *Pseudomonas aeruginosa* OxyR-C199D mutant, in which the sensing cysteine residue is replaced with aspartic acid, gives us a hint as to this mechanism (10). The crystal structure OxyR-C199D holds a H_2O_2 molecule near aspartic acid that is even bulkier than a cysteine residue, implying that H_2O_2 can also bind to the same site even after the sensing cysteine is oxidized to Cys-SOH or Cys-SO_2H. The bound H_2O_2 can eventually oxidize the cysteine to Cys-SO_3H by the same H_2O_2-driven oxidation mechanism proposed previously (10). We modeled Cys-SOH, Cys-SO_2H, and Cys-SO_3H forms based on the *P. aeruginosa* OxyR-C199D structure that contains H_2O_2 molecules (Fig. 6*A*). Steric clash was not observed around the modeled cysteine residues with modification. Moreover, the lone pair electrons of the sulfur atoms in the cysteine residues could be facing H_2O_2 within a reasonable distance for nucleophilic attack on the H_2O_2 molecule when the -SOH or -SO_2H moiety is simply rotated in the model. These findings support the idea that overoxidation at the sensing cysteine residue by H_2O_2 can occur faster than at other cysteine residues, presumably by the successive H_2O_2-driven oxidation mechanism.

Three different redox states of OxyR are determined, depending on the cellular levels of H_2O_2 as depicted in Fig. 6*B*. At low levels of H_2O_2 below the sensing level of OxyR, OxyR is maintained in the reduced state. Under the Prx2 working range of H_2O_2, a kinetic path renders the sensing cysteine in OxyR oxidized to the Cys-SOH intermediate that forms a disulfide bond with the other redox-sensitive cysteine, leading to activation of the target antioxidant genes. However, when H_2O_2 levels exceed the Prx2 working range, the Cys-SOH intermediate would be rapidly overoxidized to the Cys-SO_3H via Cys-SO_2H by H_2O_2 before making the disulfide bond. The resulting overoxidized OxyR2 turns off the production of useless Prx2. We do not yet know what happens to the overoxidized OxyR when the cellular H_2O_2 level returns to the working range. One plausible mechanism is that the overoxidized OxyR is degraded and new OxyR is synthesized, so that the cell can constantly respond to the changing environment. Given that the cellular amount of OxyR2 is very low (11), the energy needed for this process is not high.

In summary, *V. vulnificus* OxyR2 is primarily characterized as a three-state redox switch. A thiol-based sensor protein OxyR2 senses H_2O_2 and shifts to a third redox state, the overoxidized state, as a result of overoxidation of sensing cysteine residue by H_2O_2. Overoxidized OxyR2 prevents production of Prx2 where Prx2 is no longer functional and thereby saves val-

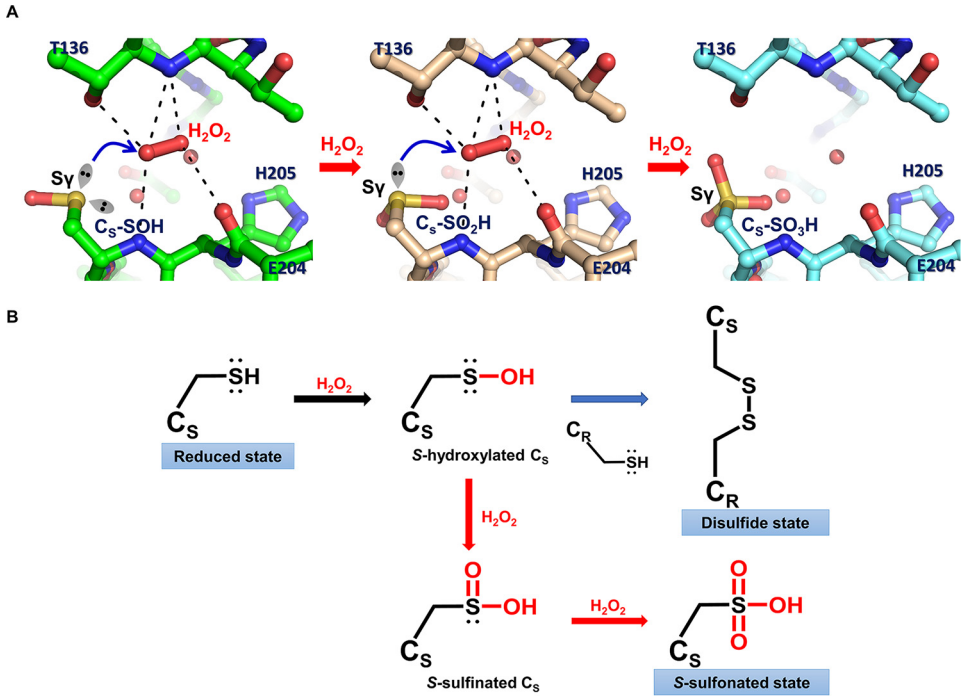

FIGURE 6. **Proposed overoxidation mechanism of OxyR.** *A*, modeled structures of OxyR, focusing on the sensing cysteine (C_S). *S*-Hydroxylated sensing cysteine (C_S-*SOH*) is oxidized by the bound H_2O_2 (*left*), resulting in *S*-sulfinated sensing cysteine (C_S-SO_2H; *middle*), which is in turn further oxidized to *S*-sulfonated sensing cysteine (C_S-SO_3H; *right*). The models were constructed based on the crystal structure of the *P. aeruginosa* OxyR-C199D variant complexed with a H_2O_2 molecule. The H_2O_2 molecule was bound by the polar interactions with the side chain and the backbone amide group of Thr^{136}, the backbone carbonyl group of Glu^{204}, and the backbone amide group of Cys^{206}, as indicated by the *dotted lines*. The lone pair of electrons are displayed as the sp^3 *orbital shapes*, and the bound water molecules are shown as *red spheres*. The *blue arrows* indicate the nucleophilic attack by Sγ of sensing cysteine on an oxygen atom of H_2O_2. *B*, schematic reaction mechanism of oxidation of sensing cysteine and the concomitant three redox states of OxyR. Sensing cysteine of OxyR in the reduced state is converted to *S*-hydroxylated sensing cysteine by H_2O_2, as a reaction intermediate (*black arrow*). *S*-Hydroxylated sensing cysteine rapidly makes a disulfide with the other redox-sensitive cysteine (C_R), resulting in the disulfide state of OxyR (*blue arrow*). Alternatively, *S*-hydroxylated sensing cysteine is further oxidized consecutively by H_2O_2 to the final *S*-sulfonated sensing cysteine in the presence of excess H_2O_2, resulting in the overoxidized state of OxyR (*red arrows*).

uable cellular resources. The DNA sequences for binding of $OxyR2_{5CA}$-C206D suggested that overoxidized OxyR2 adopts an extended conformation and turns off P_{prx2} by binding to elongated sequences masking the −35 region. Expression patterns of *prx1* and *katG* in response to various H_2O_2 levels suggested that OxyR1, a homolog of *E. coli* OxyR, also functions as a three-state redox switch, as does OxyR2.

Experimental Procedures

Bacterial Strains, Plasmids, and Culture Media—The strains and plasmids used in this study are listed in Table 1. The *V. vulnificus* strains were grown in LB medium supplemented with 2.0% (w/v) NaCl (LBS) at 30 °C. Anaerobic conditions were obtained using an anaerobic chamber with an atmosphere of 90% N_2, 5% CO_2, and 5% H_2 (Coy Laboratory Products, Grass Lake, MI). For anaerobic culture, the media were preincubated to remove dissolved O_2 in the anaerobic chamber, which was verified by adding 0.00001% (w/v) resazurin salt (Sigma) to the media as described previously (11).

Site-directed Mutagenesis of oxyR2 and Purification of Mutant OxyR2 Proteins—A mutant OxyR2 in which Cys^{206} was replaced with aspartic acid was constructed using the QuikChange® site-directed mutagenesis kit (Agilent Technologies, Loveland, CO) as described previously (11). The complementary mutagenic primers listed in Table 2 were used in conjunction with the plasmid pDY1025 (*oxyR2* cloned into a broad host-range vector pJH0311 under the *lac* promoter) to create pBANG1416 (*oxyR2*-C206D on pJH0311) (Table 1). The mutation was confirmed by DNA sequencing. *E. coli* SM10 λ *pir, tra* (23) harboring pJH0311, pDY1025, or pBANG1416 was used as a conjugal donor to the *oxyR2* mutant (OH0703). The conjugation was conducted as described previously (11).

Mutant OxyR2 proteins, OxyR2-C206S and $OxyR2_{5CA}$-C206D, were constructed and purified for MALDI-TOF MS analysis and DNA footprinting assay, respectively. Cys^{206} of OxyR2 was replaced with serine using pDY1001 (*oxyR2* on pET-28a(+) as a template) and the complementary mutagenic primers (Table 2) to result in pDY1104 (*oxyR2*-C206S on pET-28a(+)). Similarly, Cys^{206} of $OxyR2_{5CA}$ was replaced with serine using pDY1014 ($oxyR2_{5CA}$ on pET-28a(+) as a template) to result in pBANG1501 ($oxyR2_{5CA}$-C206D on pET-28a(+)) (Table 1). The resulting His_6-tagged mutant OxyR2 proteins were produced in *E. coli* BL21 (DE3) and purified by affinity chromatography using Ni^{2+}-nitrilotriacetic acid resin (Qiagen, Valencia, CA) as described previously (11).

MALDI-TOF MS Analysis—To investigate the redox state of Cys^{206} in OxyR2 *in vitro*, the full-length His_6-tagged OxyR2 and OxyR2-C206S proteins were analyzed by MALDI-TOF MS, as described previously (11, 17). Briefly, to reduce the proteins, 20 μg of proteins in a reaction buffer (20 mM Tris (pH 7.4), 0.3 M KCl, 5 mM $MgCl_2$, 0.5 mM EDTA, and 10% (v/v) glycerol) were

treated with 100 mM DTT for 1 h, and then the DTT was removed by gel filtration chromatography under anaerobic conditions. To prepare oxidized proteins, reduced OxyR2 proteins were reacted with 500 μM H_2O_2 for 10 min after the DTT removal. Subsequently, the reduced cysteine residues of each reduced and overoxidized OxyR2 protein were alkylated with 50 mM iodoacetamide for 1.5 h in the dark under anaerobic conditions. Alkylated OxyR2 proteins were resolved on non-reducing SDS-PAGE, and the protein bands were excised and in-gel digested with trypsin (Sigma). Peptides were extracted from the gel pieces with 0.1% trifluoroacetic acid in 50% acetonitrile, concentrated to volumes of 10 μl using a SpeedVac concentrator (Savant Instruments Inc., Farmingdale, NY), and desalted using Zip-Tip C_{18} reverse phase peptide separation matrix (Millipore, Billerica, MA).

MALDI-TOF MS analyses were carried out on a Voyager-DE™ STR biospectrometry work station (Applied Biosystems Inc., Foster City, CA) operating in positive and negative ion reflector modes. α-Cyano-4-hydroxycinnamic acid (10 mg/ml) in 50% acetonitrile and 0.1% trifluoroacetic acid was used as a matrix. The theoretical monoisotopic masses ($[M - H]^-$ for the deprotonated form in the negative ion reflector mode or $[M + H]^+$ for the protonated form in the positive ion reflector mode) of the cleavage peptides were determined using PeptideMass software from the ExPASy proteomics server. The masses from the positive ion reflector mode were calibrated internally with known masses of autolytic trypsin peptides. However, the masses from the negative ion reflector mode were uncalibrated because the trypsin peaks were not detectable in the negative ion mode.

In Vivo Alkylation of OxyR2 and Western Blotting Analysis—The *oxyR2* mutant OH0703 with pDY1025 expressing *oxyR2* was used for Western blotting analysis of OxyR2 as described previously (11). OH0703 (pDY1025) was grown anaerobically to an A_{600} of 0.3, aliquoted to the same volume, and exposed to various concentrations of H_2O_2. To alkylate free thiols in the proteins with AMS, the cells were immediately precipitated with ice-cold TCA, and then the resulting pellets were dissolved in 50 μl of the fresh AMS buffer (15 mM AMS, 1 M Tris, 1 mM EDTA, 0.1% (w/v) SDS, pH 8.0) (11).

After incubation at 37 °C for 1 h, the same amounts of pelleted total protein were resolved on SDS-PAGE under non-reducing conditions and immunoblotted with either anti-OxyR2 or anti-OxyR2-Cys^{206}-SO_3H antibody as described previously (11). The anti-OxyR2 polyclonal antibody was prepared previously in a rabbit by using the purified His_6-tagged OxyR2 as an antigen (11). An *S*-sulfonated peptide corresponding to the active site of OxyR2, EKEHC^{206}(SO_3H)LTEHA, was synthesized and conjugated with keyhole limpet hemocyanin and then used to raise rabbit anti-OxyR2-Cys^{206}-SO_3H polyclonal antibody (AbFrontier, Seoul, South Korea).

TABLE 1
Bacterial strains and plasmids used in this study

Strains or plasmids	Relevant characteristics[a]	Reference or source
Bacterial strains		
V. vulnificus		
MO6-24/O	Clinical isolate; virulent	Laboratory collection
OH0703	MO6-24/O with *oxyR2*::*nptI*; Km^r	Ref. 11
E. coli		
SM10 λ *pir*	*thi thr leu tonA lacY supE recA*::RP4–2-Tc::Mu λ*pir*; Km^r; host for -requiring plasmids; conjugal donor	Ref. 23
BL21 (DE3)	*F*$^-$ *ompT hsdS* (rB$^-$mB$^-$) *gal* (DE3)	Laboratory collection
Plasmids		
pJH0311	0.3-kb MCS of pUC19 cloned into pCOS5; Ap^r, Cm^r	Ref. 26
pDY1025	pJH0311 with wild-type *oxyR2*; Ap^r, Cm^r	Ref. 11
pBANG1416	pJH0311 with the mutant *oxyR2* encoding OxyR2-C206D; Ap^r, Cm^r	This study
pET-28a(+)	His_6-tag fusion protein expression vector; Km^r	Novagen
pDY1001	pET-28a (+) with wild-type *oxyR2*; Km^r	Ref. 11
pDY1104	pET-28a (+) with the mutant *oxyR2* encoding OxyR2-C206S; Km^r	This study
pDY1014	pET-28a (+) with the mutant *oxyR2* encoding $OxyR2_{5CA}$; Km^r	Ref. 11
pBANG1501	pET-28a (+) with the mutant *oxyR2* encoding $OxyR2_{5CA}$-C206D; Km^r	This study

[a] Ap^r, ampicillin-resistant; Cm^r, chloramphenicol-resistant; Km^r, kanamycin-resistant.

TABLE 2
Oligonucleotides used in this study

Name	Oligonucleotide Sequence (5′→3′)[a,b]	Use
For mutagenesis		
OXYR2C206D-F	GGAAAAAGAGCATGATCTGACTGAACACGCGGTGTCGG	Construction of OxyR2-C206D mutant
OXYR2C206D-R	CCGACACCGCGTGTTCAGTCAGATCATGCTCTTTTTCC	
OXYR2C206S-F	GGAAAAAGAGCATAGTCTGACTGAACAC GCGGTGTCGGCC	Construction of OxyR2-C206S mutant
OXYR2C206S-R	GGCCGACACCGCGTGTTCAGTCAGACTATGCTCTTTTTCC	
For quantitative real-time PCR		
PRX2QRT-F	GTTGCTTTCCGTGGCTCTTTCC	Expression of *prx2*
PRX2QRT-R	TACTTCGCCGTGCTTCTGGTG	
OXYR2QRT2-F	GCCCAGTCTGAAGCAGTTACACTATC	Expression of *oxyR2*
OXYR2QRT2-R	GAGAGGACAGCCGATCAACTCTTC	
PRX1QRT-F	TACCCAGCGGACTTCACTTTCG	Expression of *prx1*
PRX1QRT-R	TGACACTGAGTACACTTCCACACC	
KATGQRT-F	CGTTCCGTTTGCAGCAGGTC	Expression of *katG*
KATGQRT-R	CCAGTTGCGGAAGCCATCTG	
For DNA footprinting		
PRX2P02-F	GCAGAGTAATAAGATAGTGTAACTGC	Amplification of *prx2* upstream region
PRX2P02-R	CCTACTAGTACCATTTTTTTGCTCC	

[a] The oligonucleotides were designed using the *V. vulnificus* MO6-24/O genomic sequence (GenBank™ accession numbers CP002469 and CP002470).
[b] Regions of oligonucleotides not complementary to the corresponding genes are underlined.

ELISA—The Cys^{206}-SH peptide EKEHC^{206}(SH)LTEHA and its *S*-sulfonated form, Cys^{206}-SO_3H peptide EKEHC^{206}(SO_3H)-LTEHA, were synthesized (AbFrontier) and used to analyze the binding specificity of anti-OxyR2-Cys^{206}-SO_3H antibody. The microtiter 96-well plates were coated with 100 μl of each of the synthetic peptides (1 μg/ml) for overnight at 4 °C and blocked with the blocking buffer (2% skim milk in PBS with 20 mM 2-mercaptoethanol) for 2 h to prevent a nonspecific binding. After the blocking buffer was disposed, various concentrations of anti-OxyR2-Cys^{206}-SO_3H antibody in 100 μl of the blocking buffer were added to each well and reacted for 2 h. When needed, the peptides were added to the reaction along with the antibody as binding competitors.

Then the wells were reacted with HRP-conjugated goat anti-rabbit IgG (0.2 μg/ml) (AbFrontier) for 2 h. For the colorimetric development of HRP, 3,3′,5,5′-tetramethylbenzidine solution (0.0075% (w/v), Sigma) was added and reacted for 1 min. The reaction was stopped by adding 100 μl of 2 M H_2SO_4. Absorbance at 450 nm (A_{450}) was recorded to measure the amount of anti-OxyR2-Cys^{206}-SO_3H antibody in each well using an Infinite^{TM} M200 microplate reader (Tecan, Männedorf, Switzerland). The wells were washed between each step of the reaction either with TBST-M (50 mM Tris, 150 mM NaCl, 0.1% Tween 20, 20 mM 2-mercaptoethanol) before anti-OxyR2-Cys^{206}-SO_3H antibody was added or with TBST (50 mM Tris, 150 mM NaCl, 0.1% Tween 20) after the antibody was added. All reactions were carried out at room temperature.

RNA Purification and Transcript Analysis—Total cellular RNAs from the cultures grown anaerobically to an A_{600} of 0.3 or aerobically to an A_{600} of 0.5 were isolated using RNAprotect® bacteria reagent and an RNeasy® minikit (Qiagen). When necessary, the cultures were exposed to H_2O_2 for 3 min and then harvested. For quantitative real-time PCR, cDNA was synthesized using the iScript^{TM} cDNA synthesis kit (Bio-Rad), and real-time PCR amplification of the cDNA was performed using the Chromo 4 real-time PCR detection system (Bio-Rad) with pairs of primers listed in Table 2. Relative expression levels of the specific transcripts were calculated using the 16S rRNA expression level as the internal reference for normalization (24).

DNA Footprinting Assay—DNA footprinting assays were conducted as described previously (11). The 260-bp upstream region of P_{prx2}, extending from −246 to +14, was amplified by PCR using [γ-^{32}P]ATP-labeled PRX2P02-R and unlabeled PRX2P02-F primers (Table 2). The labeled 260-bp DNA (25 nM) probe was incubated with various concentrations of purified $OxyR2_{5CA}$-C206D for 30 min at 30 °C in a 20-μl reaction mixture containing 1× binding buffer (25 mM Tris-Cl (pH 8.0), 25 mM KCl, 6 mM $MgCl_2$, 0.5 mM EDTA, 10% (v/v) glycerol, 0.05% (v/v) Tween 20, and 50 μg/ml BSA). The DNA-protein complexes were digested with 0.1 units of DNase I for 30 s at 30 °C. After ethanol precipitation, the digested DNA products were resolved on a sequencing gel alongside sequencing ladders of the same 260-bp upstream region of P_{prx2}. The gels were visualized using a phosphor imager analyzer (BAS1500, Fuji Photo Film Co. Ltd., Tokyo, Japan).

Modeling of OxyR2 Structures—To construct models for an overoxidized OxyR2 structure containing a H_2O_2 molecule, we used the coordinates of the full-length OxyR-C199D variant from *P. aeruginosa* (Protein Data Bank code 4X6G), where an H_2O_2 molecule is bound near the mutated Asp^{199} residue corresponding to Cys^{206} of OxyR2. The Asp^{199} residue in the structure was changed to Cys-SOH, Cys-SO_2H, or Cys-SO_3H using the program COOT (25). Then -SOH, -SO_2H, or -SO_3H was rotated to be suitable for the nucleophilic attack on the bound H_2O_2 molecule.

Data Analyses—Mean and S.D. were calculated from at least three independent experiments. To analyze H_2O_2 concentration-dependent expression of *prx2*, *oxyR2*, *prx1*, and *katG*, data were assessed for normal distribution and homogeneity of variance by Shapiro-Wilks' test. Data that had normal distribution were analyzed by one-way analysis of variance, and data that did not have normal distribution were analyzed by Kruskal-Wallis one-way analysis of variance on ranks. Statistical significance was assessed by the Student-Newman-Keuls method as a post hoc test using SigmaPlot version 13. Significance of differences between experimental groups was accepted at a p value of <0.05.

Author Contributions—Y.-J. B., Z.-W. L., D. K., I. J., N.-C. H., and S. H. C. designed the research; Y.-J. B., Z.-W. L., D. K., and I. J. performed the research; Y.-J. B., I. J., N.-C. H., and S. H. C. analyzed the data; and Y.-J. B., I. J., N.-C. H., and S. H. C. wrote the paper. All authors reviewed the results and approved the final version of the manuscript.

References

1. Storz, G., and Imlay, J. A. (1999) Oxidative stress. *Curr. Opin. Microbiol.* **2,** 188–194
2. Stadtman, E. R. (2001) Protein oxidation in aging and age-related diseases. *Ann. N.Y. Acad. Sci.* **928,** 22–38
3. Lemire, J. A., Harrison, J. J., and Turner, R. J. (2013) Antimicrobial activity of metals: mechanisms, molecular targets and applications. *Nat. Rev. Microbiol.* **11,** 371–384
4. Cooke, M. S., Evans, M. D., Dizdaroglu, M., and Lunec, J. (2003) Oxidative DNA damage: mechanisms, mutation, and disease. *FASEB J.* **17,** 1195–1214
5. Miller, R. A., and Britigan, B. E. (1997) Role of oxidants in microbial pathophysiology. *Clin. Microbiol. Rev.* **10,** 1–18
6. Storz, G., and Zheng, M. (2000) Oxidative stress. in *Bacterial Stress Responses* (Storz, G., and Hengge-Aronis, R. eds) pp. 44–59, American Society for Microbiology Press, Washington, D. C.
7. Dubbs, J. M., and Mongkolsuk, S. (2012) Peroxide-sensing transcriptional regulators in bacteria. *J. Bacteriol.* **194,** 5495–5503
8. Choi, H., Kim, S., Mukhopadhyay, P., Cho, S., Woo, J., Storz, G., and Ryu, S. E. (2001) Structural basis of the redox switch in the OxyR transcription factor. *Cell* **105,** 103–113
9. Zheng, M., Aslund, F., and Storz, G. (1998) Activation of the OxyR transcription factor by reversible disulfide bond formation. *Science* **279,** 1718–1721
10. Jo, I., Chung, I. Y., Bae, H. W., Kim, J. S., Song, S., Cho, Y. H., and Ha, N. C. (2015) Structural details of the OxyR peroxide-sensing mechanism. *Proc. Natl. Acad. Sci. U.S.A.* **112,** 6443–6448
11. Kim, S., Bang, Y. J., Kim, D., Lim, J. G., Oh, M. H., and Choi, S. H. (2014) Distinct characteristics of OxyR2, a new OxyR-type regulator, ensuring expression of Peroxiredoxin 2 detoxifying low levels of hydrogen peroxide in *Vibrio vulnificus*. *Mol. Microbiol.* **93,** 992–1009
12. Toledano, M. B., Kullik, I., Trinh, F., Baird, P. T., Schneider, T. D., and Storz, G. (1994) Redox-dependent shift of OxyR-DNA contacts along an extended DNA-binding site: a mechanism for differential promoter selection. *Cell* **78,** 897–909

13. Heo, Y. J., Chung, I. Y., Cho, W. J., Lee, B. Y., Kim, J. H., Choi, K. H., Lee, J. W., Hassett, D. J., and Cho, Y. H. (2010) The major catalase gene (*katA*) of *Pseudomonas aeruginosa* PA14 is under both positive and negative control of the global transactivator OxyR in response to hydrogen peroxide. *J. Bacteriol.* **192,** 381–390
14. Tseng, H. J., McEwan, A. G., Apicella, M. A., and Jennings, M. P. (2003) OxyR acts as a repressor of catalase expression in *Neisseria gonorrhoeae*. *Infect. Immun.* **71,** 550–556
15. Lee, C., Lee, S. M., Mukhopadhyay, P., Kim, S. J., Lee, S. C., Ahn, W. S., Yu, M. H., Storz, G., and Ryu, S. E. (2004) Redox regulation of OxyR requires specific disulfide bond formation involving a rapid kinetic reaction path. *Nat. Struct. Mol. Biol.* **11,** 1179–1185
16. Tao, K., Fujita, N., and Ishihama, A. (1993) Involvement of the RNA polymerase α subunit C-terminal region in co-operative interaction and transcriptional activation with OxyR protein. *Mol. Microbiol.* **7,** 859–864
17. Bang, Y. J., Oh, M. H., and Choi, S. H. (2012) Distinct characteristics of two 2-Cys peroxiredoxins of *Vibrio vulnificus* suggesting differential roles in detoxifying oxidative stress. *J. Biol. Chem.* **287,** 42516–42524
18. Janek, K., Wenschuh, H., Bienert, M., and Krause, E. (2001) Phosphopeptide analysis by positive and negative ion matrix-assisted laser desorption/ionization mass spectrometry. *Rapid Commun. Mass Spectrom.* **15,** 1593–1599
19. Groitl, B., and Jakob, U. (2014) Thiol-based redox switches. *Biochim. Biophys. Acta* **1844,** 1335–1343
20. Seo, S. W., Kim, D., Szubin, R., and Palsson, B. O. (2015) Genome-wide reconstruction of OxyR and SoxRS transcriptional regulatory networks under oxidative stress in *Escherichia coli* K-12 MG1655. *Cell Rep.* **12,** 1289–1299
21. Klauck, E., and Hengge, R. (2012) σS-controlling networks in *Escherichia coli.* in *Bacterial Regulatory Networks* (Filloux, A., ed) pp. 1–26, Caister Academic Press, Norfolk, United Kingdom
22. Dong, T., Joyce, C., and Schellhorn, H. E. (2008) The role of RpoS in bacterial adaptation. in *Bacterial Physiology: A Molecular Approach* (El-Sharoud, W., ed) pp. 313–337, Springer, Berlin
23. Miller, V. L., and Mekalanos, J. J. (1988) A novel suicide vector and its use in construction of insertion mutations: osmoregulation of outer membrane proteins and virulence determinants in *Vibrio cholerae* requires *toxR*. *J. bacteriol.* **170,** 2575–2583
24. Lim, J. G., Bang, Y. J., and Choi, S. H. (2014) Characterization of the *Vibrio vulnificus* 1-Cys peroxiredoxin Prx3 and regulation of its expression by the Fe-S cluster regulator IscR in response to oxidative stress and iron starvation. *J. Biol. Chem.* **289,** 36263–36274
25. Emsley, P., and Cowtan, K. (2004) Coot: model-building tools for molecular graphics. *Acta Crystallogr. D Biol. Crystallogr.* **60,** 2126–2132
26. Goo, S. Y., Lee, H. J., Kim, W. H., Han, K. L., Park, D. K., Lee, H. J., Kim, S. M., Kim, K. S., Lee, K. H., and Park, S. J. (2006) Identification of OmpU of *Vibrio vulnificus* as a fibronectin-binding protein and its role in bacterial pathogenesis. *Infect. Immun.* **74,** 5586–5594